Journal of Neuroinflammation

RESEARCH

Open Access

Ubiquitination-mediated upregulation of glycolytic enzyme MCT4 in promoting astrocyte reactivity during neuroinflammation

Luting Yang[1*†], Chunqing Hu[1†], Xiaowen Chen[1†], Mengru Sun[1†], Jie Zhang[1], Zhe Feng[1], Tingting Cui[1], Ruyi Zhu[1], Xin Zhang[1], Yanxin Xiao[1], Ye Gong[2], Yang Yang[1], Qian Zhang[1], Yaling Zhang[1] and Yaping Yan[1*]

Abstract

One of the histopathological hallmarks of neuroinflammatory diseases such as multiple sclerosis (MS) is the emergence of astrocyte reactivity. Accumulating evidence suggests that excessive glycolysis may lead to astrocyte reactivity and contribute to neuroinflammatory responses. However, the intricate mechanisms underlying astrocyte metabolic reprogramming towards glycolysis remain largely unknown. Here, we conducted in vitro experiments using primary astrocytes and in vivo studies in an experimental autoimmune encephalomyelitis (EAE) mouse model of multiple sclerosis (MS). We observed increased astrocytic expression of MCT4, a key glycolytic regulator, in EAE mice. MCT4 enhanced astrocyte reactivity through promoting glycolysis and proliferation, mediated primarily by activation of the NF-κB and c-Myc signaling pathways. Notably, we report a novel regulatory mechanism in which the E3 ubiquitin ligase TRIM7 regulates MCT4 levels via ubiquitination. In mice, blockade of astrocyte MCT4 expression by intracerebroventricular injection of lentivirus alleviated disease severity of EAE mice. The results suggest that targeting glycolysis, specifically through the inhibition of MCT4 expression, might be effective in reducing astrocyte reactivity, neuroinflammation and demyelination occurring in MS and relating neuroinflammatory diseases.

Keywords Experimental autoimmune encephalomyelitis, Astrocyte, Ubiquitination, Proliferation, Glycolysis

Introduction

The importance of astrocytes in the central nervous system (CNS) is evidenced by their critical roles ranging from providing structural and metabolic support to synapse regulation. Astrocyte reactivity, including diverse forms of changes that differ from their homeostatic state, can exert either neurotoxic or protective roles in a context-dependent manner in demyelinating disorders such as multiple sclerosis (MS), neuromyelitis optica spectrum disorders (NMOSD), as well as in neurodegenerative conditions such as Alzheimer's disease and Parkinson's disease [1, 2]. In preclinical studies, targeting astrocytes has emerged as a promising strategy for treating neurological disorders [3].

†Luting Yang, Chunqing Hu, Xiaowen Chen and Mengru Sun contributed equally to this work.

*Correspondence:
Luting Yang
yangluting@snnu.edu.cn
Yaping Yan
yaping.yan@snnu.edu.cn
[1]Key Laboratory of the Ministry of Education for Medicinal Resources and Natural Pharmaceutical Chemistry, National Engineering Laboratory for Resource Development of Endangered Crude Drugs in Northwest of China, College of Life Sciences, Shaanxi Normal University, Xi'an 710119, China
[2]Department of Experimental Surgery, Tangdu Hospital, Air Force Medical University, Xi'an 710038, China

Astrocytes are the most abundant glial cells that are primarily dedicated to maintaining homeostasis in the CNS. Through in-depth investigations and high-throughput sequencing techniques, astrocytes have been revealed to display heterogeneity in a context- and disease-dependent manner [4]. Astrocytes are highly plastic in response to CNS injury, disease and infection during which they undergo a process termed "reactive astrogliosis", "astrocyte activation" or "astrocyte reactivity" [2]. While astrocyte reactivity initially serves to preserve CNS homeostasis during pathology, various mechanisms result in loss of homeostatic astrocytic functions and reprogram astrocytes as instigators of neuropathology [1]. MS, the most common demyelinating autoimmune disease, is characterized by inflammatory demyelinating lesions and axonal damage. Accumulating evidence has corroborated that astrocyte reactivity plays a central role in MS progression by aggravating CNS inflammation, blood–brain barrier (BBB) disruption, and demyelination [5]. Numerous studies have identified signaling pathways including NF-κB, STAT3 and Notch that are involved in astrocyte reactivity in MS [6, 7]. Nevertheless, the identification of novel targets and mechanisms that selectively drive astrocyte reactivity remains critical for both elucidating disease pathogenesis and developing targeted therapeutic strategies.

Astrocytes metabolize glucose to provide energy for neurons to function properly. The energy demand is predominantly met by aerobic glycolysis, also known as Warburg effect, which is accompanied by increased release of lactate [8]. Enhanced glycolytic activity observed in astrocytes of MS patients and EAE has been implicated in driving astrocyte reactivity, the release of proinflammatory cytokines and neurotrophic factors, and subsequent demyelination and neuronal loss in CNS [9, 10]. These findings suggest that enhanced aerobic glycolysis serves as a pathogenic mechanism driving astrocyte reactivity in EAE and MS. Building upon our previous demonstration that nuclear translocation of the glycolytic rate-limiting enzyme PKM2 led to enhanced aerobic glycolysis and astrocyte reactivity in EAE [11], we hereby focused on other pivotal glycolysis-related enzymes. Lactate, the end-product of aerobic glycolysis, leads to intracellular acidosis and cell damage [12]. Astrocytes export lactate to survive the accumulation of lactate via its transporters, namely monocarboxylate transporters (MCTs) [13]. Among the four isoforms of MCTs, MCT1 and MCT4 are expressed in astrocytes [14]. Given the substantial lactate production via aerobic glycolysis in astrocytes during MS and EAE, along with the absence of acidosis in MS patients, we further postulated an upregulation of MCTs expression in astrocytes during EAE.

Post-translational modifications (PTMs), including ubiquitination, SUMOylation and acetylation, play a pivotal role in regulating protein stability, subcellular localization and protein-protein interaction. Traditionally recognized as the primary PTM that targets proteins for degradation, ubiquitination has emerged as a key regulator of a myriad of biological processes. Ubiquitination is catalyzed by a cascade of enzymes in which E3 ubiquitin ligases confer substrate specificity. TRIM7 is an E3 ubiquitin ligase that has not been extensively studied. Most studies have pinpointed its role in mediating antiviral responses and in tumorigenesis [15, 16]. However, it remains unclear whether TRIM7 regulates metabolic processes or targets metabolic enzymes such as MCTs, PKM2, PFKP, and GLUT1.

Our study identified a pathological upregulation of MCT4 in astrocytes during EAE. Beyond its established role in lactate export, we uncovered the non-metabolic function of MCT4 in promoting astrocyte reactivity. Notably, we demonstrated that MCT4 protein stability is controlled by TRIM7-mediated ubiquitination. Furthermore, we observed a reduction in TRIM7 expression in astrocytes of EAE mice. To validate the pathophysiological significance of MCT4, our findings revealed that astrocyte-specific knockdown of MCT4 significantly attenuated EAE severity in vivo. By shedding light on the involvement of MCT4 in astrocyte reactivity in EAE, our study offers new insights for potential therapeutic targets in the clinical treatment of multiple sclerosis.

Results

MCT4 level is increased in astrocytes of EAE

Previous findings have shown an upregulation of both MCT1 and MCT4 in active MS lesions [17], we next sought to determine their relative expressions in astrocytes of EAE mice. Immunofluorescence staining revealed MCT1 expression in both astrocytes and neurons (Fig. S1A, S1E and F). However, quantitative analysis showed no significant increase in MCT1 levels in astrocytes of EAE mice compared with naïve controls (Fig. S1B). Moreover, in primary astrocytes stimulated with supernatants from MOG_{35-55}-stimulated splenocytes of EAE (MOG_{sup}), which was previously shown to elicit a T-cell response in the acute stage of EAE [11, 18], mRNA and protein levels of MCT1 were not increased (Fig. S1C and D). We next focused on the expression of MCT4. When compared to naïve mice, we observed an increased fluorescence intensity of MCT4 in astrocytes during different phases of EAE (onset, peak, and chronic) mice (Fig. 1A and B). Furthermore, the proportion of MCT4-positive astrocytes and MCT4 area coverage were elevated in EAE mice (Fig. 1C and D). To corroborate these findings, primary astrocytes were cultured with either MOG_{sup} or the inflammatory stimuli TNF-α and IL-1β, which are linked to MS and EAE pathology [19]. Expectedly, mRNA levels of MCT4 were upregulated in

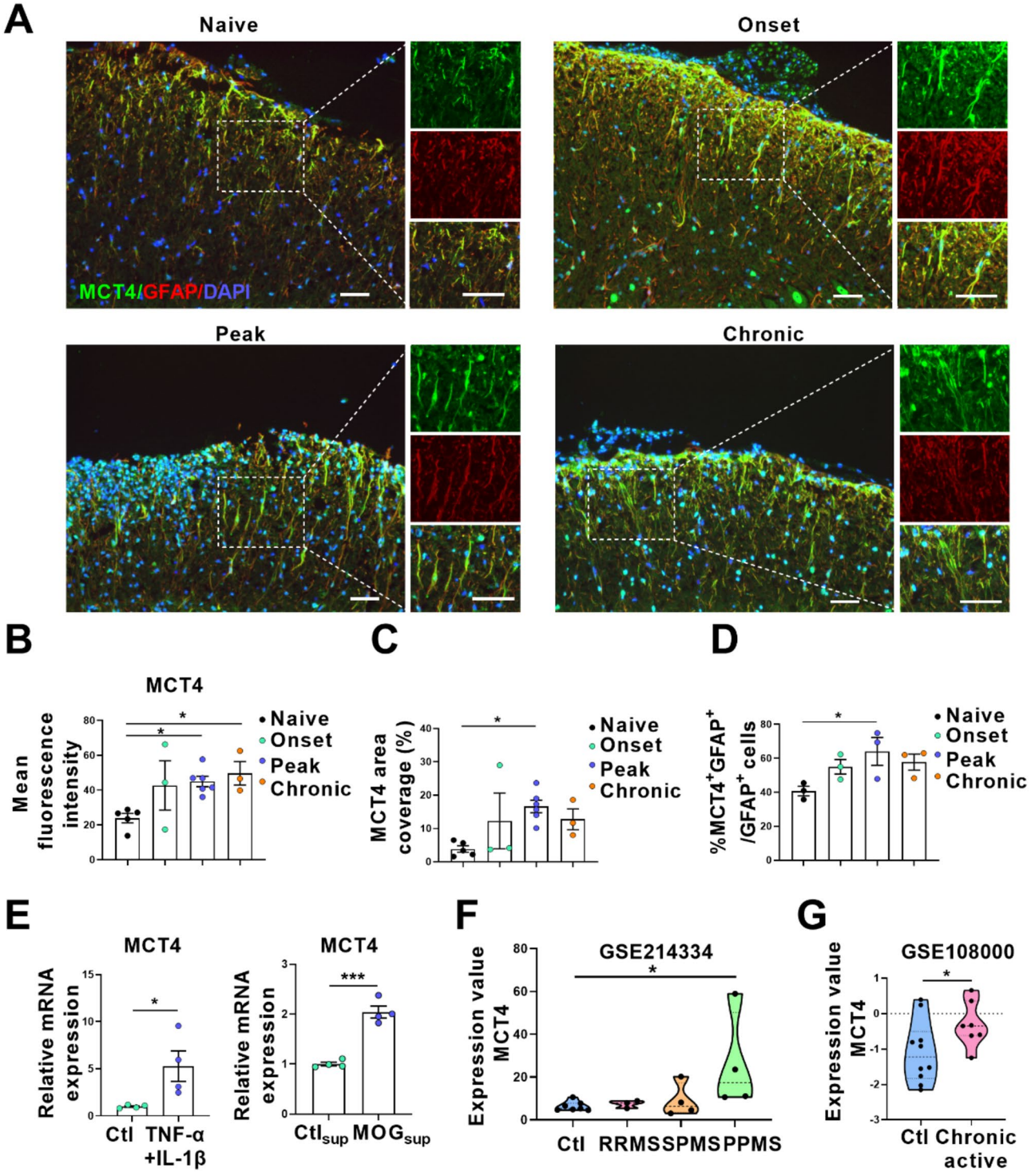

Fig. 1 (See legend on next page.)

astrocytes stimulated with MOG_{sup} or TNF-α and IL-1β (Fig. 1E). To analyze the expression of MCT4 in patients from multiple sclerosis, we screened GEO datasets. Data from two independent GEO datasets revealed upregulated expression of MCT4 in normal-appearing white matter (GSE214334, Fig. 1F) [20] and rim of chronic active MS lesions (GSE108000, Fig. 1G) [21]. Altogether, these data demonstrate that MCT4 expression is elevated in astrocytes of EAE mice.

(See figure on previous page.)

Fig. 1 MCT4 expression is upregulated in astrocytes of EAE mice. **(A)** Representative images (low and high magnification) showing immunofluorescence staining of MCT4 in the astrocytes (GFAP) in the spinal cords from naive, EAE onset (score 1; Day 7–17 p.i.), peak (score ≥ 3; Day 14–24 p.i.), and chronic (score ≥ 2; Day 21–26 p.i.) mice. **(B)** Quantification of mean fluorescence intensity of MCT4 in the spinal cord of EAE onset ($n = 3$), peak ($n = 6$), chronic ($n = 3$) and naive ($n = 5$) mice. **(C)** Quantification of MCT4 positive area coverage in spinal cord in different groups of mice. EAE onset ($n = 3$), peak ($n = 6$), chronic ($n = 3$) and naive ($n = 5$). **(D)** Quantification of $MCT4^+GFAP^+$ cells in the total number of $GFAP^+$ cells in EAE onset ($n = 3$), peak ($n = 3$), chronic ($n = 3$) and naive ($n = 3$) mice. **(E)** qRT-PCR analysis of MCT4 in primary astrocytes treated alone or with TNF-α and IL-1β (left), or treated with splenocytes supernatants of control mice (Ctl_{sup}) or with splenocytes supernatants of MOG_{35-55}-induced EAE mice (MOG_{sup}) for 24 h. **(F)** Analysis of MCT4 mRNA expression in normal-appearing white matter from relapse-remitting multiple sclerosis (RRMS), primary progressive MS (PPMS), secondary progressive MS (SPMS) and non-MS control tissue from GEO dataset GSE214334. **(G)** Analysis of MCT4 mRNA expression in control tissue and rim of chronic active MS lesions from GSE108000. Scale bar: 50 µm. Data are represented as mean ± SEM. $^*P < 0.05$, $^{***}P < 0.001$, using one-way ANOVA with Dunnett's multiple comparison test (**B**, **C**, **D** and **F**), using unpaired t test (**E** and **G**)

MCT4 promotes proliferation and glycolysis in astrocytes

Astrocytes are increasingly recognized as pivotal cells that contribute to the development of MS lesions [22]. In light of metabolic and functional changes observed in astrocytes during MS, characterized by heightened glycolysis and astrocyte proliferation, we sought to investigate whether MCT4 plays a role in these aforementioned pathological processes. The knockdown of MCT4 resulted in decreased lactate production and glucose consumption in astrocytes (Fig. 2A, Fig. S2A and B). To further validate the inhibitory effects of MCT4 blockade, we employed α-cyano-4-hydroxy-cinnamic acid (CHCA), a broad-spectrum monocarboxylate transporter (MCT) blocker that has been widely utilized as an inhibitor of MCT4 in previous studies [23, 24]. Consistently, application of MCT4 inhibitor CHCA significantly reduced lactate production and glucose consumption in TNF-α and IL-1β-stimulated astrocytes (Fig. 2B). qRT-PCR analysis further revealed that glycolysis-related enzymes, such as GLUT1 and HK2, were markedly downregulated following knockdown or treatment with MCT4 inhibitor in astrocytes (Fig. 2D and E). Additionally, lactate production was increased upon overexpression of MCT4 (Fig. 2C, Fig. S2C and D). These results suggested that MCT4 promoted glycolysis in astrocytes.

We then evaluated whether MCT4 could regulate astrocyte proliferation. As illustrated in Fig. 2F, MCT4 inhibitor dramatically reduced the proportion of EdU positive cells in TNF-α and IL-1β stimulated astrocytes. Consistently, knockdown with either shMCT4-1 or shMCT4-2 significantly decreased the proportion of EdU-positive cells (Fig. 2G). Moreover, EdU assays revealed that MCT4 overexpression promoted astrocyte proliferation (Fig. 2H). Collectively, these findings indicate that MCT4 has the potential to stimulate both proliferation and glycolysis in astrocytes.

MCT4 induces activation of NF-κB and c-Myc signaling in astrocytes

To delineate the mechanisms underlying MCT4-mediated proliferation and glycolysis, we screened for signaling pathways associated with these biological processes. A key signaling pathway that governs MS transcriptional signatures is c-Myc [25]. Moreover, NF-κB orchestrates astrocyte transcriptional networks associated with CNS inflammation [26]. Therefore, we focused on these two signaling pathways.

In TNF-α and IL-1β stimulated astrocytes, both MCT4 knockdown and treatment with the MCT4 inhibitor CHCA markedly reduced the phosphorylation of p65 (Fig. 3A-B, Fig. S4A and B). These results indicated that MCT4 could potentially promote the activation of NF-κB signaling pathway. In addition to NF-κB, results from western blotting showed that MCT4 knockdown also inhibited activation of c-Myc signaling pathway, which is crucial in regulating cell proliferation, cell cycle and metabolic reprogramming (Fig. 3C) [27]. Moreover, in TNF-α and IL-1β stimulated astrocytes, CHCA treatment led to reduced level of phospho-c-Myc (Fig. 3D). To explore whether MCT4 interacts directly with NF-κB and c-Myc to promote their activation, we performed immunoprecipitation. Our results revealed that MCT4 directly interacts with c-Myc, p50 and p65 subunits of NF-κB. In contrast, no detectable interaction was observed between MCT4 and other tested proteins, including STAT3 and IκBα (Fig. S3).

We next sought to assess whether MCT4-mediated activation of NF-κB and c-Myc was linked to increased proliferation and glycolysis of astrocytes. For this purpose, MCT4-overexpressing astrocytes were treated with c-Myc inhibitor 10,058-F4 or NF-κB inhibitor JSH-23. As shown in Fig. 3E and F, increase in astrocyte proliferation induced by MCT4 overexpression was significantly rescued by treatment with c-Myc or NF-κB inhibitor. Consistently, the increased level of lactate production induced by MCT4 overexpression was partially restored by c-Myc or NF-κB inhibitor (Fig. 3G). Thus, our data show that MCT4 activates c-Myc and NF-κB signaling pathways to promote the proliferation and glycolysis of astrocytes.

E3 ligase TRIM7 interacts with MCT4 and its expression is decreased in astrocytes of EAE

To dissect the molecular mechanisms by which MCT4 promotes the activation of NF-κB and C-myc, we used immunoprecipitation to analyze MCT4 interacting

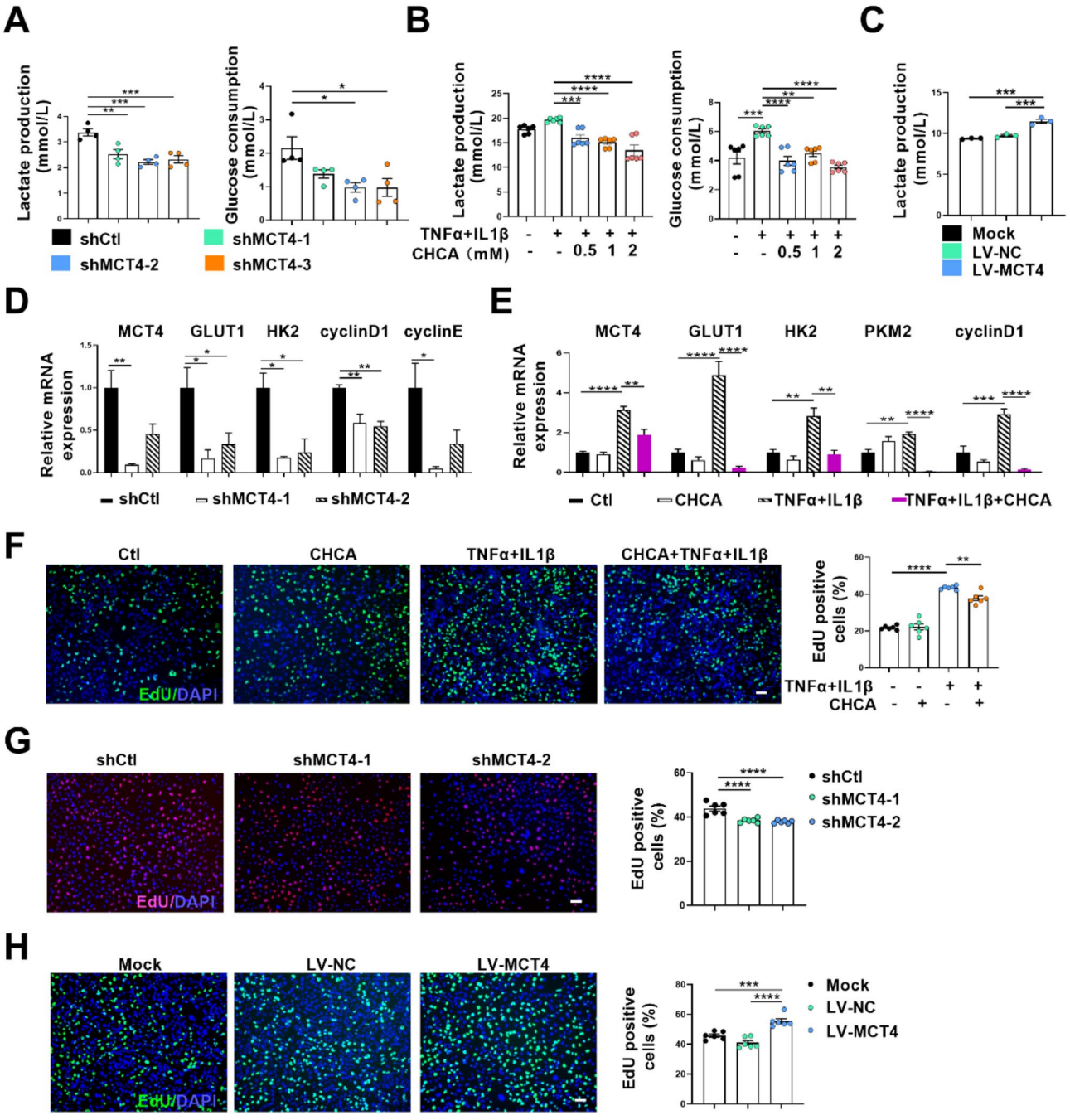

Fig. 2 MCT4 promotes astrocyte glycolysis and proliferation. **(A)** Analysis of glucose consumption and lactate production levels in MCT4-knockdown astrocytes (shMCT4) and control astrocytes (shCtl). **(B)** Primary astrocytes were treated with MCT4 inhibitor CHCA for 24 h, followed by stimulation with 50 ng/mL TNF-α and IL-1β for 24 h. Glucose consumption and lactate production levels were measured. **(C)** Analysis of lactate production levels in MCT4-overexpressed astrocytes (LV-MCT4), control astrocytes (LV-NC), and non-treated astrocytes (mock). **(D)** qRT-PCR analysis of MCT4, GLUT1, HK2, Cyclin D1 and Cyclin E in MCT4-knockdown astrocytes and control astrocytes. **(E)** Effect of MCT4 inhibitor CHCA (1 mM) on the mRNA expression of MCT4, GLUT1, HK2, PKM2 and Cyclin D1 in TNF-α and IL-1β-stimulated astrocytes. **(F)** Effect of MCT4 inhibitor CHCA on the proliferation of TNF-α and IL-1β stimulated astrocytes was measured by EdU assay. For quantification of EdU, 6 fields were included for each group. **(G)** Cell proliferation was measured in MCT4 knockdown and control astrocytes. EdU^+ cells were quantified. **(H)** Cell proliferation was measured in mock, control-lentivirus and MCT4-overexpressed astrocytes by EdU incorporation assay. EdU^+ cells were quantified by Image-Pro Plus. Scale bar: 100 μm. Data are represented as mean ± SEM. $^*P < 0.05$, $^{**}P < 0.01$, $^{***}P < 0.001$, $^{****}P < 0.0001$ using one-way ANOVA with Dunnett's multiple comparison test

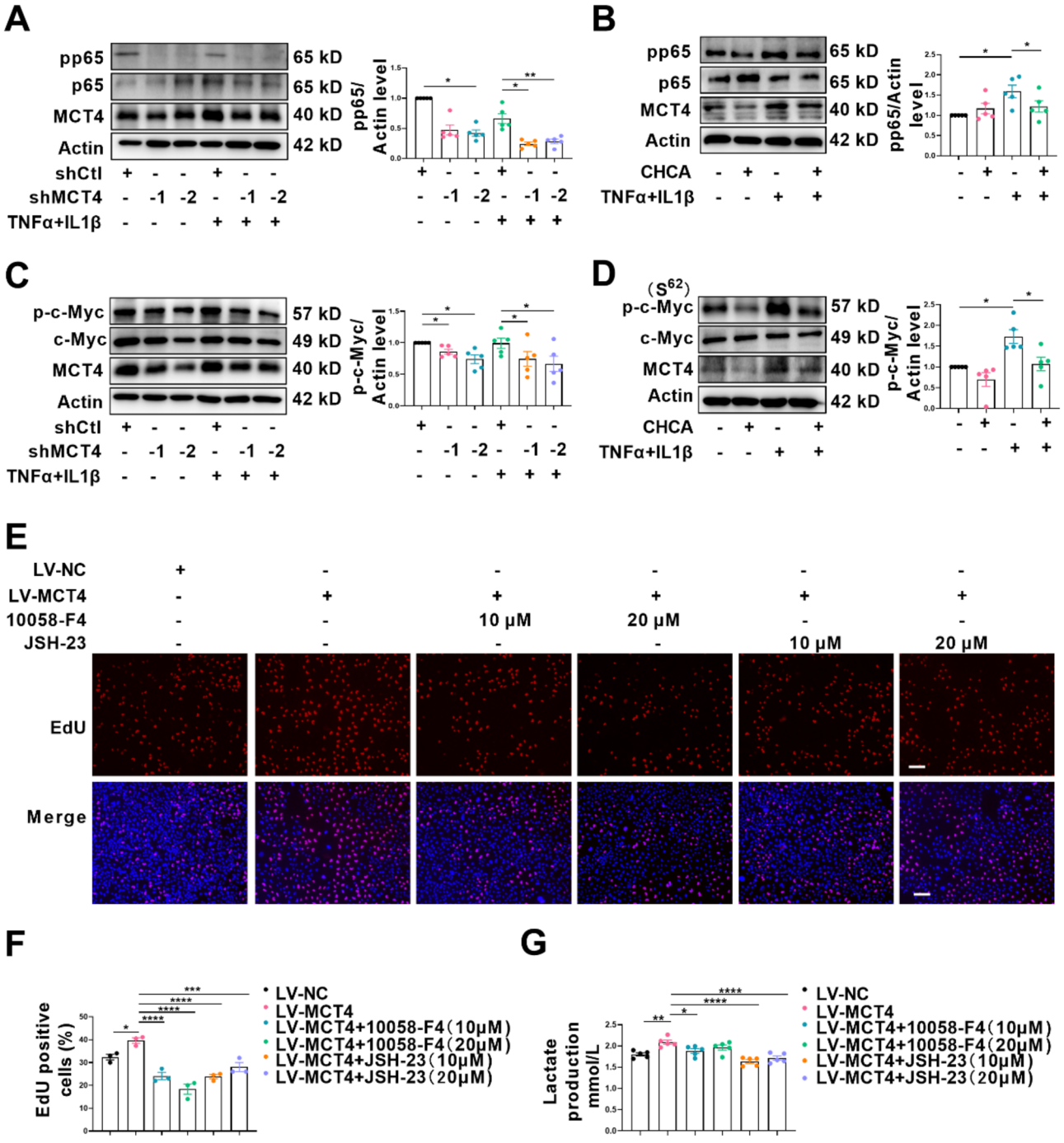

Fig. 3 MCT4 promotes cell proliferation and glycolysis via activation of NF-κB and c-Myc pathway. **(A)** Western blotting analysis of NF-κB pathway activation in MCT4-knockdown and control astrocytes, cultured alone, or with 50 ng/mL TNF-α and IL-1β for 24 h. The protein level of phospho-p65 is normalized to β-actin. **(B)** Effect of MCT4 inhibitor CHCA on the expression of phosphorylated p65 in NF-κB pathway was measured by western blotting. Primary astrocytes were pretreated with 1 mM CHCA for 24 h, followed by stimulation with TNF-α and IL-1β for 24 h. The protein level of phospho-p65 is normalized to β-actin. **(C)** Western blotting analysis of phosphorylated c-Myc and total c-Myc in MCT4-knockdown and control astrocytes. The protein level of phospho-c-Myc is normalized to β-actin. **(D)** Effect of MCT4 inhibitor CHCA on activation of c-Myc signaling was measured by western blotting. The protein level of phospho-c-Myc is normalized to β-actin. **(E)** Effect of c-Myc inhibitor and NF-κB inhibitor on the proliferation of astrocytes was measured by EdU assays. Cells were treated with NF-κB inhibitor JSH-23 for 2 h, or with c-Myc inhibitor 10,058-F4 for 24 h at indicated concentration. **(F)** EdU^+ cells were quantified in each group indicated. **(G)** Effect of c-Myc inhibitor and NF-κB inhibitor on lactate production of astrocytes were measured. Scale bar: 100 μm. Data are from at least 3 independent experiments **(A-D)**. Data are represented as mean ± SEM. $^*P < 0.05$, $^{**}P < 0.01$, $^{***}P < 0.001$, $^{****}P < 0.0001$ using one-way ANOVA with Dunnett's multiple comparison test

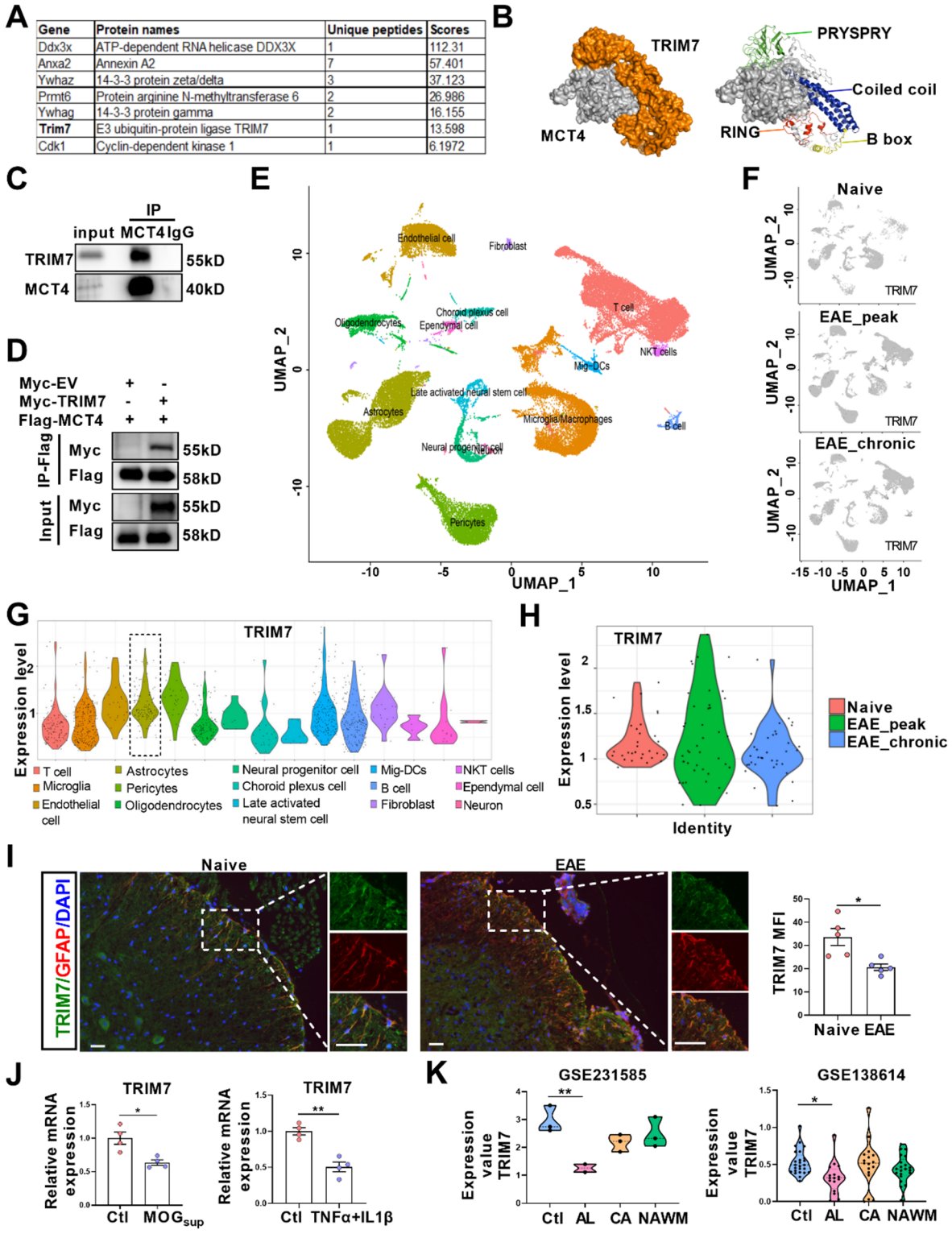

Fig. 4 (See legend on next page.)

proteins. Following immunoprecipitation and mass spectrometry analysis in primary astrocytes, a series of proteins were shown to be potentially interact with MCT4. Notably, TRIM7—a member of the E3 ubiquitin ligase family, was detected in the MCT4 immunoprecipitates (Fig. 4A). Given that ubiquitination, one of the fundamental post-translational modifications that regulates protein stability, localization, interaction and activation

(See figure on previous page.)

Fig. 4 E3 ubiquitin ligase TRIM7 interacts with MCT4 and its expression is downregulated in astrocytes of EAE mice. **(A)** List of MCT4 binding proteins identified by mass spectrometry. Primary astrocytes overexpressed with MCT4-GFP were immunoprecipitated with GFP. **(B)** Molecular docking of TRIM7 and MCT4 performed by ZDOCK. Different domains of TRIM7, including RING (red), Coiled coil (blue) and PRY-SPRY (green) were predicted to interact with MCT4. Pymol software was used to display the docking results. **(C)** Immunoprecipitation with anti-MCT4 showed endogenous binding between TRIM7 and MCT4 in primary astrocytes. **(D)** Astrocytes were transfected with Myc-tagged TRIM7 and Flag-tagged MCT4, or with Myc-tagged empty vector and Flag-tagged MCT4. Immunoprecipitation with anti-Flag showed exogenous binding between TRIM7 and MCT4. **(E-H)** Single-cell RNA-seq profiles from control and EAE mice (peak and chronic phase) CNS tissues. **(E)** UMAP of CNS cells colored by cell types from mice with EAE. **(F)** Expression of TRIM7 in different cell types from naive and EAE mice. **(G)** Violin plots displaying the expression of TRIM7 across the cell types identified. **(H)** Violin plots displaying the expression of TRIM7 at peak, chronic phases from naive and EAE mice in astrocytes. **(I)** Representative images of immunofluorescence staining of TRIM7 (green) and GFAP (red) in spinal cords of naive and EAE mice. Quantification of mean fluorescence intensity of TRIM7 in the spinal cords of naive ($n=5$) and EAE ($n=5$) mice. **(J)** qRT-PCR analysis of TRIM7 mRNA expression in primary astrocytes treated with MOG_{sup} (left) or 50 ng/mL TNF-α and IL-1β for 24 h. **(K)** RNA-seq analysis of TRIM7 expression in the white matter of MS patient (AL: active lesion, CA: chronic active, NAWM: normal-appearing white matter) and controls from GEO dataset GSE231585 and GSE138614. Scale bar: 50 μm. Data are represented as mean ± SEM. $^{*}P<0.05$, $^{**}P<0.01$ using unpaired t-test

[28], we therefore investigated whether TRIM7 interacted with MCT4. Molecular docking analysis confirmed the conformational interaction between TRIM7 and MCT4 (Fig. 4B). Subsequent immunoprecipitation experiments demonstrated robust endogenous binding between TRIM7 and MCT4 in primary astrocytes (Fig. 4C). We next constructed a Flag-tagged MCT4 lentivirus and Myc-tagged TRIM7 lentivirus, co-immunoprecipitation revealed the exogeneous interactions between TRIM7 and MCT4 (Fig. 4D).

To highlight the pathological significance of this interaction, we analyzed TRIM7 expression in EAE mice. Single-cell RNA sequencing revealed widespread TRIM7 expression across various cell types (Fig. 4E-G). Further analysis in astrocytes showed that TRIM7 expression was downregulated in astrocytes during the peak phase of EAE compared to naive mice (Fig. 4H). Immunofluorescence confirmed the reduced TRIM7 expression in astrocytes of EAE mice (Fig. 4I). Specificity of immunofluorescence staining was verified by isotype controls (Fig. S5). Moreover, treatment with either MOG_{sup} or TNF-α and IL-1β significantly decreased TRIM7 mRNA expression in primary astrocytes (Fig. 4J). To evaluate whether TRIM7 exhibits similarly reduced expression in MS patients, we analyzed GEO datasets. Data from GSE231585 and GSE138614 showed that compared with controls [29, 30], TRIM7 mRNA levels were downregulated in active lesions of MS patients (Fig. 4K). Taken together, our data newly uncover the decreased expression of TRIM7 in astrocytes during EAE, and demonstrate an interaction between TRIM7 and MCT4.

TRIM7 promotes the degradation of MCT4 via ubiquitination

Based on the aforementioned data concerning the inverse expression pattern observed between MCT4 and TRIM7 in astrocytes during EAE, we reasoned that TRIM7 potentially modulated the stability of MCT4. For this, we constructed TRIM7-overexpressing and knockdown lentiviruses. Knockdown of TRIM7 increased the protein level of MCT4, whereas overexpression of TRIM7 led to a reduction in MCT4 protein level (Fig. 5A and B). As ubiquitination mediated by TRIM7 is involved in protein degradation, we assessed whether TRIM7 affected the protein stability of MCT4. Cycloheximide-based assays demonstrated sustained MCT4 expression over a 48-hour period in control cells, whereas in astrocytes overexpressing TRIM7, the half-life of MCT4 was shortened to approximately 48 h (Fig. 5C). Furthermore, cells incubated with proteasome inhibitor MG132 could block the degradation of MCT4 induced by TRIM7 overexpression, suggesting that degradation of MCT4 could be regulated by the ubiquitin proteasome pathway (Fig. 5D). To determine the specific types of ubiquitination involved, primary astrocytes were co-transfected with Flag-MCT4 and Myc-TRIM7 or Myc-empty vector, followed by co-immunoprecipitation assays. Our findings indicated that TRIM7 overexpression significantly increased K48-linked polyubiquitination of MCT4, which typically leads to protein degradation (Fig. 5E).

TRIM7 restricts MCT4-mediated proliferation and glycolysis of astrocytes

To delve deeper into the biological significance of TRIM7-MCT4 axis, we reconstituted a regulatory system by knocking down both TRIM7 and MCT4 with shTRIM7 and shMCT4. Knockdown of TRIM7 increased the proportion of EdU positive astrocytes, whilst this effect was markedly restored by knockdown of MCT4 together with TRIM7, indicating that TRIM7 restricts MCT4-mediated proliferation of astrocytes (Fig. 5F and G). Furthermore, TRIM7 knockdown increased the level of glucose consumption and lactate production, whereas knockdown of MCT4 together with TRIM7 partially abolished the increase in glycolysis caused by TRIM7 knockdown (Fig. 5H). These results indicated that TRIM7 repressed the MCT4-mediated proliferation and glycolysis of astrocytes.

MCT4 knockdown in astrocytes alleviates EAE

Given the verified pivotal role of MCT4 in promoting pathological changes of astrocytes, we next evaluated in vivo whether interfering with MCT4 in astrocytes affects EAE induction. Mice were administered with lentivirus

targeting MCT4 in astrocytes (shMCT4) or control lentivirus (shCtl) via intracerebroventricular injection 3 days before immunization. Knockdown of MCT4 in astrocytes during prevention stage (administration before disease onset) alleviated disease severity and delayed disease onset (Fig. 6A). To assess the pathological changes, spinal cords of shCtl and shMCT4-treated mice with EAE were harvested. As revealed by H&E and LFB staining, inflammation and demyelination were less pronounced in shMCT4-treated EAE mice (Fig. 6B and C). The in vivo efficiency of shMCT4 was verified by immunofluorescence, which showed a significant reduction in MCT4 expression following lentivirus injection (Fig. 6D). Demyelination lesions were measured by MBP staining. Compared with shCtl-treated EAE group, proportion of intact myelin was increased in shMCT4-treated EAE mice (Fig. 6E and F). Activation of glial cells, including microglia and astrocytes, are involved the progression of EAE. Therefore, the effect of MCT4 knockdown on glial cell activation was investigated. Immunostaining of the astrocyte marker GFAP and the microglia marker IBA1 was reduced in both the white matter and gray matter of shMCT4-treated EAE mice (Fig. 6E and F).

Furthermore, to verify the biological effect of MCT4 knockdown on the proliferation of astrocytes, Ki67 immunostaining in astrocytes were performed. Consistent with in vitro results, the knockdown of MCT4 reduced the proliferation of astrocytes in EAE mice (Fig. S6A). Further analysis with phosphorylated p65 and c-Myc showed a slight decrease in the activation of NF-κB in astrocytes of EAE mice (Fig. S6B and C). Altogether, these results indicate that knocking down MCT4 in astrocytes holds potential as a therapeutic approach in MS.

Discussion

Despite the growing body of evidence supporting the role of aerobic glycolysis in various neuroinflammatory diseases, the cellular mechanisms underlying this metabolic rewiring and their pathophysiological roles in these disorders remain to be fully elucidated. Here, we uncovered an upregulated expression of MCT4, but not MCT1, in astrocytes during EAE. We further demonstrated that MCT4 played a key role in promoting astrocytic glycolysis and proliferation via NF-κB and c-Myc signaling pathways, contributing to astrocyte reactivity. Most importantly, we identified an E3 ubiquitin ligase TRIM7, that was downregulated in astrocytes during EAE. TRIM7 potentially interacted with MCT4 and induced its degradation. Finally, we showed that astrocyte-specific knockdown of MCT4 mitigated the EAE severity in vivo (Fig. 7).

Metabolic rewiring towards glycolysis was the prominent metabolic change identified in astrocytes of MS and EAE [31]. Our previous work demonstrated the critical role of PKM2, a rate-limiting glycolytic enzyme, in promoting aerobic glycolysis in astrocytes during EAE [11]. We built upon this evidence to investigate other glycolysis-related enzymes to gain a comprehensive understanding of the mechanisms underlying this metabolic change in MS and EAE. Increased glycolysis is characterized by elevated level of lactate that released into the extracellular space. Given that MCT1 and MCT4 represent the primary MCT family members mediating lactate transport in astrocytes, we initially assessed their expression profiles in EAE [32]. The observed upregulation of MCT4 in astrocytes of EAE mice, but not MCT1, underscores our rationale for focusing our attention on MCT4. Indeed, knockdown or inhibition of MCT4 reduced lactate release by astrocyte. Collectively, these findings extend our previous work demonstrating altered subcellular localization and dysregulated expression of glycolysis-related enzymes represent key mechanisms driving aerobic glycolysis in EAE astrocytes.

Previously, pathological role of MCT4 in macrophages has been identified in MS. The prominent expression of MCT4 enhanced glycolysis and transmigration of macrophages in EAE [23]. Given that MCT4 expression is elevated in glycolytic cells and enhanced glycolytic activity has been documented in various immune cells of MS, including monocytes, macrophages, T cells and astrocytes, it is plausible that MCT4 contributes to the metabolic reprogramming and activation of these immune cells [9]. Therefore, further investigations to elucidate the role of MCT4 in various immune cells would shed light on the importance of metabolic alterations in the global pathophysiology of MS.

Although MCT4 has been extensively studied in the context of metabolic processes, its non-metabolic functions remain poorly understood. MCT4 overexpression is associated with tumor growth and can serve as an indicator of poor prognosis for patients with cervical cancer, colorectal carcinoma, gastric cancer and lung adenocarcinoma [33, 34]. In this study, we uncovered the non-metabolic function of MCT4 in promoting astrocyte proliferation. Specifically, we corroborated that MCT4 promoted proliferation and glycolysis of astrocytes through mechanisms centered on the activation of NF-κB and c-Myc signaling. These two signaling pathways orchestrate a myriad of biological processes including cell proliferation. The major mechanism of NF-κB in cell proliferation involves transcriptionally inducing the expression of cyclins. For instance, NF-κB-dependent upregulation of cyclin D1 is crucial for the proliferation of smooth muscle cell [35]. Another widely investigated mechanism involves the interplay between NF-κB and other signaling pathways, notably AKT and STAT3 [36]. In prostate cancer, IL-6, the product of NF-κB, was

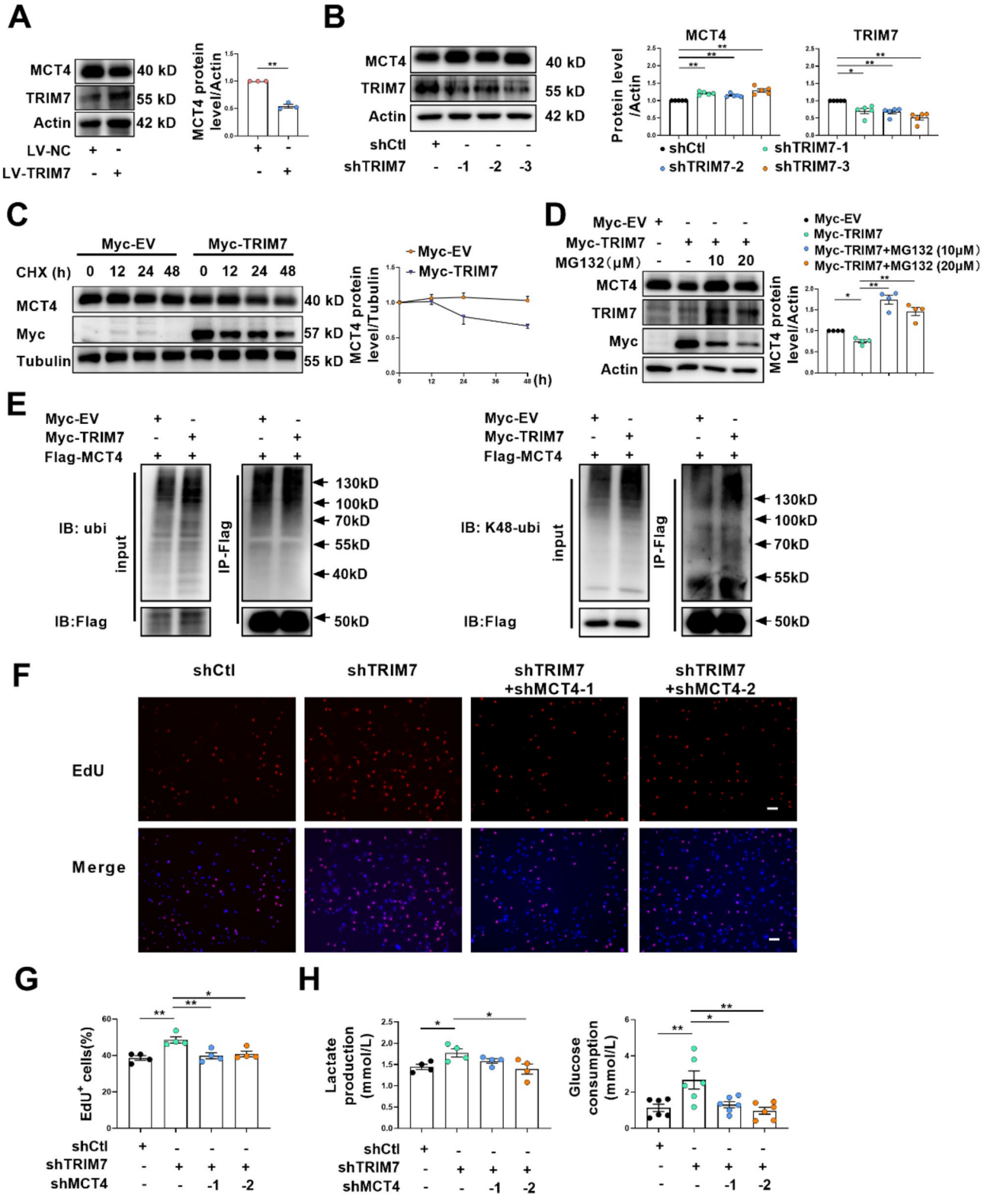

Fig. 5 (See legend on next page.)

(See figure on previous page.)

Fig. 5 TRIM7 restricts MCT4-mediated proliferation and glycolysis of astrocyte via ubiquitination. **(A)** Western blotting analysis and quantification of MCT4 protein level in TRIM7-overexpressed astrocytes and control astrocytes. **(B)** Western blotting analysis and quantification of MCT4 and TRIM7 protein level in TRIM7-knockdown and control astrocytes. **(C)** MCT4 protein stability was measured in control (Myc-EV) and TRIM7-overexpressed (Myc-TRIM7) astrocytes by cycloheximide (CHX) assays. Cells were treated with 20 μM CHX for the time indicated. (**D**) Astrocytes overexpressed with TRIM7 were treated with MG132 for 12 h. Protein level of MCT4, TRIM7 were analyzed by western blotting. **(E)** Immunoprecipitation assay showed that TRIM7 promoted the K48-linked ubiquitination of MCT4. Cells were transfected with Myc-EV and Flag-MCT4, or Myc-TRIM7 and Flag-MCT4, immunoblot analysis of total ubiquitination, K48-linked ubiquitination of Flag-tagged MCT4. **(F)** EdU assay evaluate the proliferation in control astrocytes, astrocytes knocked down with TRIM7, or astrocytes knocked down with TRIM7 and MCT4. **(G)** EdU positive cells were counted in each group in (**F**). **(H)** Lactate production and glucose consumption were detected in control astrocytes, astrocytes knocked down with TRIM7, or astrocytes knocked down with TRIM7 and MCT4. Scale bar: 100 μm. Data are from at least 3 independent experiments (**A-D**). Data are represented as mean ± SEM. $^{*}P < 0.05$, $^{**}P < 0.01$, $^{***}P < 0.001$, using one-way ANOVA with Dunnett's multiple comparison test (**B**, **D**, **G** and **H**) or paired t test (**A**)

able to activate STAT3, and this NF-κB/IL-6/STAT3 axis further facilitated prostate cancer proliferation [37]. Additionally, c-Myc was a transcription factor and a key regulator of cell cycle and cellular proliferation [27]. Many CDK genes and cyclins are upregulated by c-Myc, whereas the negative regulator of cell cycle including p15, p21 and p27 are downregulated by c-Myc [38]. Previous studies have shown that MCT4 overexpression phosphorylates p65 and promotes its nuclear translocation, leading to activation of NF-κB in intestinal epithelial cell [39]. In line with these findings, we observed MCT4-mediated activation of both NF-κB and c-Myc signaling in astrocytes. Furthermore, MCT4 was found to interact directly with p50/p65 subunits of NF-κB and c-Myc. However, detailed mechanism underlying the impact of this interaction on the activation of these pathways remains to be determined. A potential explanation could be that MCT4 induces conformational changes in NF-κB and c-Myc proteins, thereby enhancing their interactions with kinases and subsequently promoting downstream signaling pathways.

Another intriguing finding is the identification of ubiquitination-dependent regulatory mechanism that controls MCT4 expression in astrocytes. While numerous studies have evolved around the regulation of MCT4 at the transcriptional level, the knowledge regarding how MCT4 is controlled at the post-translational level remains limited. SUMOylation by FBW7 and β-TRCP led to increased protein stability of MCT4 [40]. E3 ubiquitin ligase SYVN1-mediated ubiquitination regulated MCT4 subcellular distribution, thereby enhancing its membrane localization for glycolysis-related functions [34]. Here, we identified TRIM7 as a potential E3 ubiquitin ligase of MCT4, as evidenced by mass spectrometry analysis in astrocytes. Primarily, endogenous and exogenous binding between TRIM7 and MCT4 was confirmed by immunoprecipitation in astrocytes. Further, overexpression of TRIM7 was found to promote the K48-linked ubiquitination of MCT4, the most well-established canonical signal for proteasomal degradation [41]. These results suggested TRIM7 as a bona fide E3 ubiquitin ligase for MCT4. TRIM7 is a member of the E3 ubiquitin ligase family, primarily recognized for its involvement in mediating antiviral immune responses. To date, its substrates encompass viral proteins such as enteroviruses [15, 42], Zika virus [43], and SARS-CoV-2 [15]. Additionally, proteins involved in tumor growth and ferroptosis, including NF-κB p65, SLC7A11, BRMS1, SRC and RACO-1, were identified as bona fide substrates of TRIM7 [16, 44–47]. Apart from a study reporting that TRIM7 enhanced RACO-1 protein stability via K63-linked polyubiquitination [47], in most cases, TRIM7 attached a K48-linked polyubiquitin chain to its substrate and induced proteasome-directed protein degradation. Extending previous findings, our study characterized MCT4 as a novel substrate of TRIM7. However, whether TRIM7 could mediate the ubiquitination of other metabolic-related enzymes, such as GLUT1, LDHA, PKM and HK2, remains to be elucidated. Our observations suggest that ubiquitination is a crucial mechanism that modulates the aberrant expression of MCT4 in astrocytes in neurological diseases.

To delve deeper into the cell-specific role of MCT4 and to explore therapeutic potential of MCT4 interference in EAE, we performed intracerebroventricular (i.c.v.) injections of lentivirus vectors harboring an astrocyte-specific GFAP promoter. Consistent with our previous research, which successfully knocked down TRIM21, Act1, and IFN-γ in astrocytes [11, 48, 49], injection of shMCT4 effectively suppressed MCT4 expression in astrocytes in the spinal cord of EAE mice. Notably, knockdown of MCT4 in astrocytes prior to immunization delayed the onset of EAE and reduced disease severity. This effect, together with reduced neuroinflammation and enhanced remyelination, paved the way for translational research aimed at modulating MCTs for the treatment of neurological diseases.

In conclusion, our findings underscore the significance of MCT4 upregulation in stimulating astrocytic glycolysis and proliferation, ultimately resulting in astrocyte reactivity. MCT4 was found to undergo a ubiquitination-dominated mechanism for orchestrating its protein stability and function. Collectively, this study identified a novel TRIM7-mediated regulatory mechanism of MCT4 and proposed glycolysis-related enzymes as potential therapeutic targets for neuroinflammatory diseases.

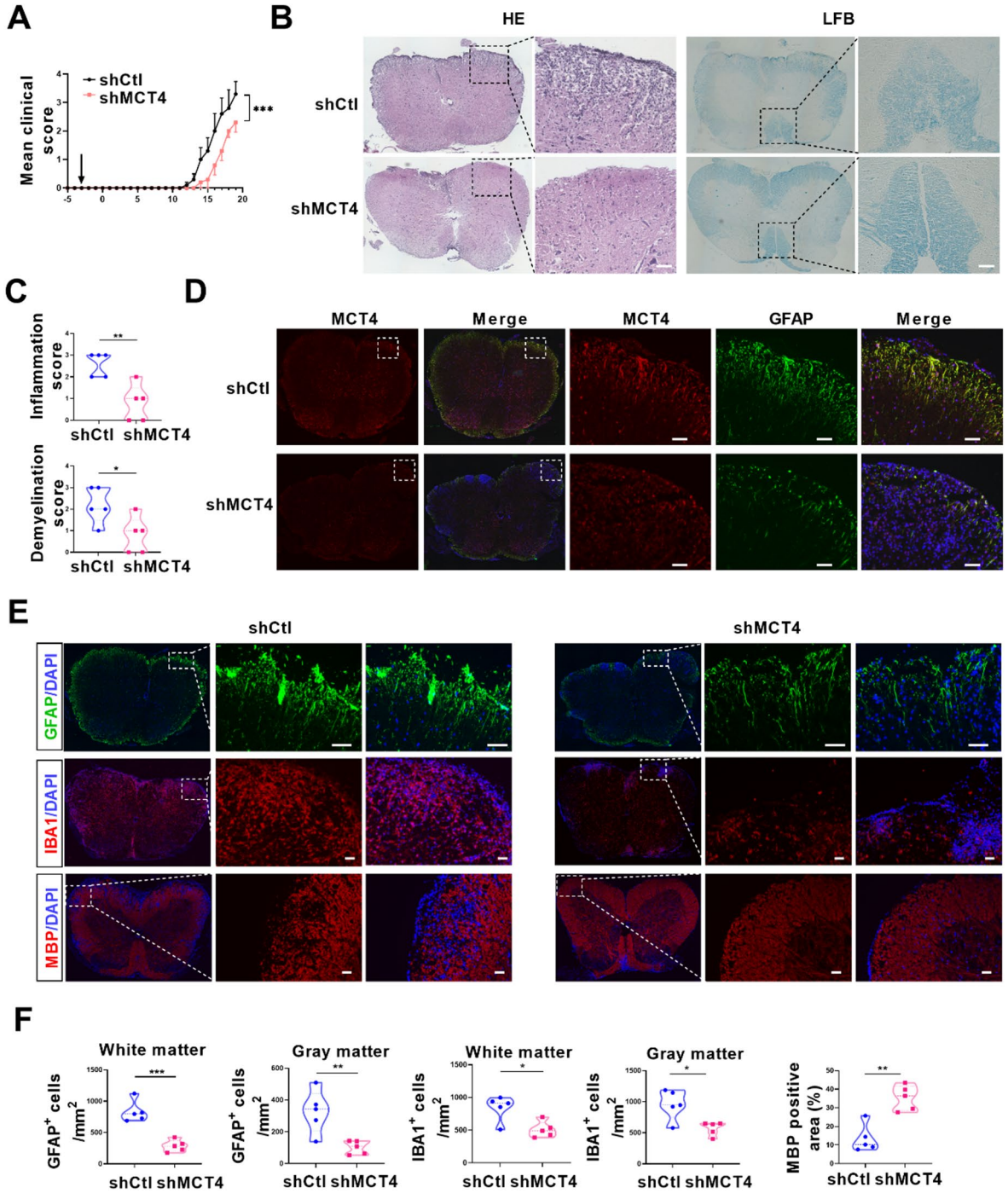

Fig. 6 Intracerebroventricular injection of shMCT4 decreases disease severity during EAE. C57BL/6 mice were injected i.c.v with 1×10^7 IU shMCT4 or control lentivirus (shCtl) 3 days before immunization. Mice were sacrificed at day 19 p.i. and spinal cords were harvested. **(A)** Disease was scored daily on a 0 to 5 scale. $n=5$ for each group. **(B)** Representative images (low and high magnification) of hematoxylin and eosin (**H**&**E**) and Luxol fast blue (LFB) staining, respectively. **(C)** Scoring of inflammation (**H**&**E**) and demyelination (LFB) on a 0–3 scale. **(D)** Verification of in vivo MCT4 knockdown efficiency by immunofluorescence in shCtl and shMCT4-treated EAE mice. **(E)** Immunostaining of GFAP, IBA1 and MBP in spinal cord sections of shCtl and shMCT4-treated EAE mice. **(F)** Quantification of GFAP positive cells/mm^2, IBA1 positive cells/mm^2 in both the white matter and gray matter. MBP positive area was measured in the white matter of the spinal cord using Image-Pro Plus. The measured areas included 3 to 5 fields per group. i.c.v., intracerebroventricular; p.i., postimmunization. Scale bar: 50 μm. Data are represented as mean ± SEM. *$P<0.05$; **$P<0.01$; ***$P<0.001$, as determined by two-way ANOVA analysis (**A**) or unpaired Student's t test (**C** and **F**)

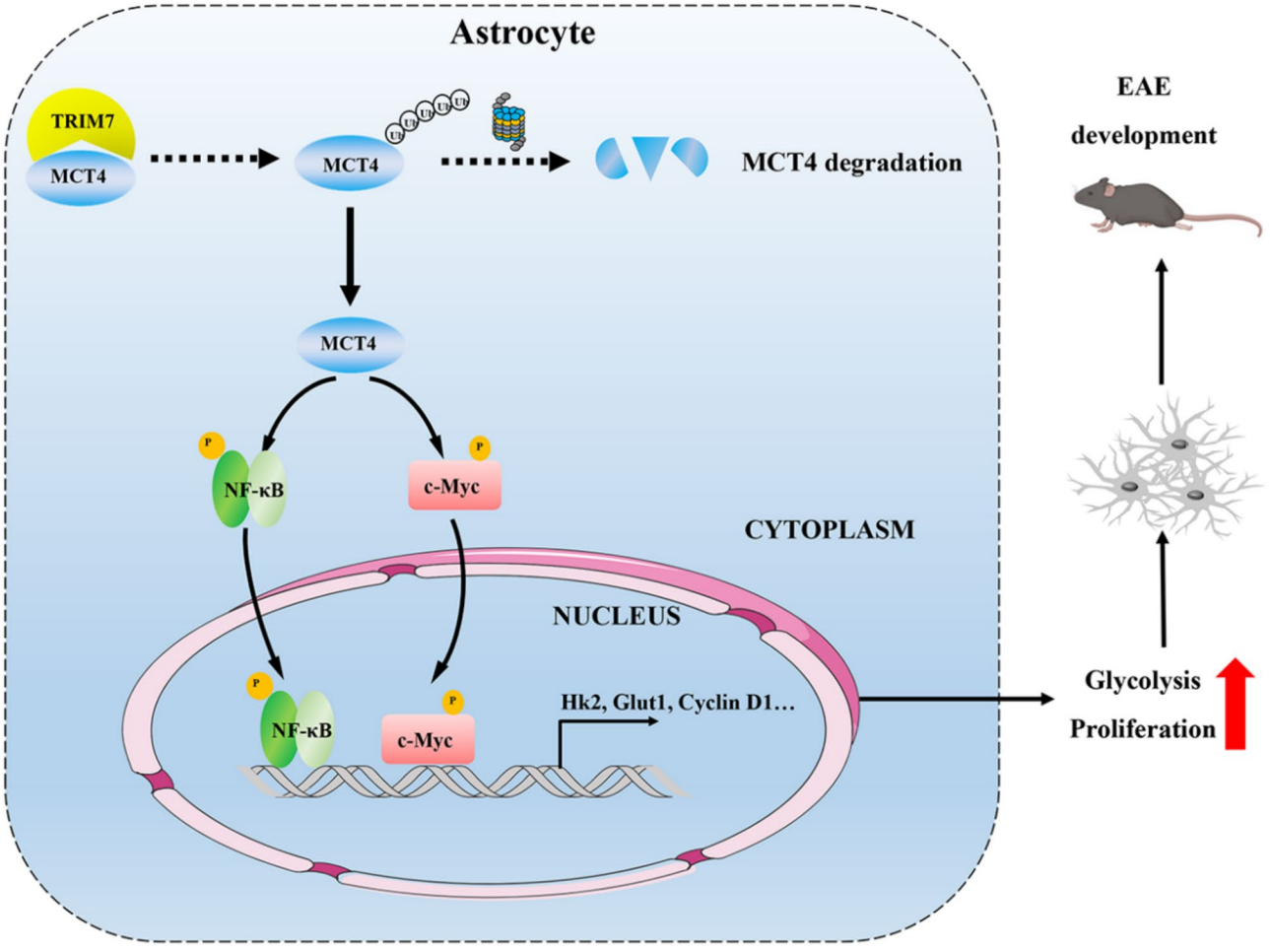

Fig. 7 Schematic representation of the proposed TRIM7-MCT4 axis in astrocyte reactivity during EAE. During MS and EAE, downregulated expression of E3 ubiquitin ligase TRIM7 reduced the ubiquitin-proteasome pathway dependent degradation of MCT4. Increased MCT4 interacted with NF-κB and c-Myc, promoting the phosphorylation and nuclear translocation of NF-κB and c-Myc. The activation of the aforementioned pathways further facilitated the activation of astrocytes via promoting astrocytic glycolysis and proliferation during EAE

Materials and methods

EAE induction

Six to eight week-old female C57BL6/J mice were purchased from Xi'an Ke aoke Biotechnology Co., Ltd. All animal experiments complied with Committee for Research and Animal Ethics of Shaanxi Normal university, and in accordance with the approved institutional regulations and guidelines (No. 2024 – 179). Mice were randomized and EAE induction was performed as previously described [11]. Briefly, mice were immunized with 200 μg myelin oligodendrocyte glycoprotein peptide 35–55 ($MOG_{35–55}$, GenScript, Nanjing, China) emulsified in CFA (Sigma, US) supplemented with 10 mg/mL heat-killed Mycobacterium tuberculosis H37Ra (Becton Dickinson, MD, USA). A total of 200 μL emulsion was subcutaneously injected at 2 sites into neck and back. 200 ng pertussis toxin (List Biological Laboratories, CA, USA) was intraperitoneally (i.p.) injected on day 0 and 2 post-immunization (p.i.). Clinical signs of EAE were monitored daily on a scale of 0–5. 0, no clinical symptoms; 1, paralyzed tail; 2, paralysis of one hind limb; 3, paralysis of two hind limbs; 4, paralysis of trunk; 5, death. Mice that did not develop symptoms of EAE were excluded from the analysis.

In vivo injection of lentivirus

For in vivo injection of control lentivirus and lentivirus that expressed MCT4-specific short hairpin RNA (shMCT4) in astrocytes, mice were anaesthetized and placed on a stereotaxic frame. A microsyringe was placed and 1×10^7 IU/mouse lentivirus was injected intracerebroventricularly (i.c.v.): 2.0 mm lateral, 1.0 mm caudal to bregma, and 2.5 mm below the skull surface. 20 μL lentivirus was administrated at a rate of 1 μL/min. The syringe was left in place for 10 min before slowly withdrawn from the brain.

Histological analysis

Spinal cord sections were placed in 4% paraformaldehyde and then paraffin embedded. 6-μm thick sections were cut and placed on slides. Paraffin-embedded sections were dewaxed with xylene, and placed in decreasing graded concentrations of alcohol for 5 min each. Sections were then dyed with hematoxylin for 5 min, washed and exposed to eosin for 5 min. Finally, sections were dehydrated in increasing grades of alcohol, cleared in xylene and then mounted. For LFB staining, sections were deparaffinized as described above and soaked in LFB staining solution (Servicebio, Wuhan, China) at 56 °C for 2 h. Excess staining was rinsed off with 95% alcohol. Slides were differentiated in 0.05% lithium carbonate for 20 s and then placed in 75% ethyl alcohol. Sections were then dehydrated and mounted with neutral resin.

Isolation of primary astrocytes and astrocytes treatment in vitro

Primary astrocytes were isolated from neonatal mice by using Neural Tissue Dissociation Kit (Miltenyi Biotech, Auburn, CA) as previously described [11].

Primary astrocytes were seeded on 6-well plate at a density of 2×10^5/well and cultured in DMEM supplemented with 10% FBS. Cells were treated with 50 ng/mL TNF-α (Novoprotein Scientific Inc., Shanghai, China) and IL-1β (Sino Biological Inc., Beijing, China). For the treatment with supernatant of MOG_{35-55}-stimulated splenocytes, spleen cells isolated from onset phase of EAE mice were seeded in 12-well plates at a density of 1×10^6 cells/well and stimulated with 50 μg/mL MOG_{35-55} for 3 days. Supernatant was collected and primary astrocytes were cultured with 30% supernatant supplemented with 70% DMEM.

Where indicated, cells were pretreated with MCT inhibitor CHCA (Topscience, Shanghai, China) for 24 h, followed by stimulation with TNFα and IL-1β for 24 h. Cells were treated with 10 or 20 μM NF-κB inhibitor JSH-23 (Topscience, Shanghai, China) for 2 h, or treated with 10 or 20 μM c-Myc inhibitor 10,058-F4 (Topscience, Shanghai, China) for 24 h. Cells were treated with 20 μM cycloheximide for the time indicated (CHX, Admole, Shanghai, China), or treated with 10 or 20 μM MG132 (Topscience, Shanghai, China) for 12 h.

Glucose consumption and lactate production assays

Cells were counted and seeded in 96-well plate at a density of 1×10^4/well. Cells were then starved for 12 h in serum-free DMEM containing low-glucose, and then replaced with DMEM containing 10% FBS. After indicated treatments, supernatant was collected. Glucose consumption was measured with the glucose oxidase method (Applygen Company, Beijing, China). Lactate production was measured using lactate assay kit (Nanjing Jiancheng, Bioengineering Institute, Nanjing, China) according to the manufacturer's instructions.

EdU and CCK8 assay

Cell proliferation was detected using EdU cell proliferation kit (Beyotime, CS0071S and CS0078S). Astrocytes were counted and seeded in 96-well plate at a density of 7×10^3 cells per well. After indicated treatment, EdU-488 or EdU-594 (10 μM) reagent was added to each well and incubated at 37 °C for 2 h. Cells were then fixed with 4% paraformaldehyde for 15 min, permeabilized with 0.3% Triton X-100 for 10 min, incubated with click-reaction reagent for another 30 min at room temperature in the dark, and then incubated with Hoechst 33,352 for another 10 min for nuclear staining. Images of EdU staining were observed with fluorescence microscope (Invitrogen, US).

For CCK-8 assay, cells were seeded in 96-well plate and cultured for 24 h, 48 h and 72 h separately. Then, 10 μL CCK-8 solution (DONGXI Biotechnology, Xi'an, China) was added to 96-well plates and incubated at 37 °C for 1 h. The absorbance was measured at 450 nm by microplate reader (Infinite F50, Tecan).

Lentiviral ShRNA vector construction

Lentiviral shRNA vectors were constructed as previously described [48]. Lentiviral vector backbone plasmid pLenti-GFAP-EGFP-shAct1 vector contains a 682 bp long GFAP promoter, followed by the enhanced green fluorescent protein (EGFP) which was used as the reporter gene. miR-30 based shAct1 cassette was inserted downstream of EGFP stop codon and transcribed simultaneously with EGFP. pLenti-GFAP-EGFP-shAct1 vector was digested with EcoRI and XhoI to remove the shAct cassette. Fragments containing miR-30 based shMCT4 or shTRIM7 cassette (Tsingke Technology, Beijing, China) were digested with EcoRI and XhoI. The digested fragments were ligated with the digested lentiviral backbone. Constructed vectors were verified by sequencing. Briefly, DNA fragments containing TAGTGAAGCCACAGAT GTA as the loop for shRNA targeting MCT4, TRIM7 or control sequences were cloned into GFAP-promoter containing mir-30 based vector.

Target sequences for mouse shMCT4 were as follows: shMCT4-1:5′- GCAGAAGCATTATCCAGATC T-3′, shMCT4-2:5′- GGTCTTTGTGGTGAGCTATG C-3′, shMCT4-3:5′-GCTCCCTCATTTACACCTTC T-3′. Target sequences for mouse shTRIM7 were as follows: shTRIM7-1:5′-TGCTCCATCTGCCTAGAGTT T-3′, shTRIM7-2:5′- GAAGGTACTGGAAGACTATG A-3′, shTRIM7-3:5′- GGGCAATGCAACTCAACAA-3′. Sequences for negative control shRNA was 5′- GCTGCT GGATGCAACCAAAGT-3′.

Construction of lentiviral vectors overexpression MCT4 or TRIM7

For overexpression of mouse TRIM7, primers were designed and mouse TRIM7 cDNA was amplified by polymerase chain reaction (PCR). PCR products were digested with XbaI and AgeI and cloned into multiple cloning sites of lentiviral vector pCDH-GFAP-MCS-Myc-EGFP.

For overexpression of mouse MCT4, primers were designed and MCT4 cDNA was amplified by PCR. PCR products were digested with XbaI and BamHI and cloned into multiple cloning sites of lentiviral vector pCDH-GFAP-MCS-3xFlag-EGFP.

Lentivirus transduction

Lentiviral packaging and titering were carried out as previously described [48]. For in vitro lentiviral transduction, purified astrocytes were seeded in 6-well plates at a concentration of 2×10^5/well. After culturing for 24 h to 48 h, primary astrocytes at 40-60% confluence were infected with lentiviral vectors (MOI = 10). 16 h after infection, the medium was replaced with fresh complete medium containing DMEM supplemented with 10% FBS. Infection efficiency was confirmed 72 h post-transduction by western blotting and qRT-PCR.

Real-time PCR

Total RNA was extracted by TRIzol, RNA purity and concentration were measured. cDNA was synthetized by using reverse transcription Master Premix reagent Kit (DEEYEE, Shanghai, China). The quantification of mRNA levels was determined by quantitative real-time polymerase chain reaction (qRT-PCR). qRT-PCR was carried out using SYBR Green SmArt Mix (DEEYEE, Shanghai, China) and StepOnePlus Real-time PCR system (Thermo Fisher). Primers used in this study are listed in Table S1. Relative expression levels were calculated from the threshold cycle (CT) values by using the 2-ΔΔCT method.

Immunofluorescence

Spinal cord sections were fixed with 4% paraformaldehyde for 1 day and cryo-protected with 30% sucrose solution for 72 h. Frozen transverse section of the spinal cord (7 μm thick) were cut. Slices were thawed at room temperature for 20 min, blocked with a PBS solution containing 1% BSA and 0.1% Triton X-100 for 1 h at room temperature. Tissues were then incubated overnight at 4 °C with appropriate primary antibodies (outlined in Table S2). After washing three times with PBS, slides were incubated with Alexa fluor-488 or 594-conjugated secondary antibodies (Zhuangzhibio, Xi'an, China) at dark for 1 h at room temperature. Cell nuclei were labeled with DAPI.

For immunocytochemical staining, astrocytes were plated on round cover glass and cultured in 24-well plates. After washing once with PBS, cells were fixed for 15 min in 4% paraformaldehyde, permeabilized with 0.3% Triton X-100 for 10 min and blocked with 1% BSA for 1 h at room temperature. Then, cells were incubated with appropriate primary antibodies (outlined in Table S2) overnight at 4 °C, followed by incubation with fluorescein-labeled secondary antibodies for 1 h at room temperature. After three times washes with PBS, cells were mounted using a mounting medium with DAPI (ab104139, Abcam). Images were captured by an EVOS FL Auto 2 Cell image system (Invitrogen). Mean fluorescence intensity was calculated by Image J version 1.53t.

Immunoprecipitation

Protein A/G magnetic beads (Cat#: HY-K0202, MedChemExpress, China) were washed and incubated with specified antibodies at 4 °C overnight under gentle rotation to obtain the antibody-coupled beads. Primary astrocytes cultured on 60-mm dishes were washed with ice-cold PBS and lysed with IP lysis buffer (Cat#: PR20037, Proteintech, China) containing 1% protease inhibitor cocktail (Cat#: C0001, TargetMol, China) and then centrifuged. Then, cell lysates were mixed thoroughly with antibody-coated magnetic beads and incubated at 4 °C for 2 h. Immunomagnetic beads were removed from sample and immunoprecipitates were collected by adding 1×SDS loading buffer and boiled. Immunoprecipitates were then analyzed by western blotting.

Immunoprecipitation and mass spectrometry

Primary astrocytes were infected with lentiviral vector backbone plasmid pLenti-GFAP-MCT4-EGFP. Cell lysates were immunoprecipitated with antibody against GFP. IP samples were then prepared, digested, separated and analyzed by Shanghai Bioprofile Biotechnology Co., Ltd. Briefly, after digestion, the peptide was separated by high performance liquid chromatograph (EASY-nLC 1200, Thermo Fisher Scientific, US). The chromatographic separation lasted for 60 min with specific gradient conditions. Mass spectrometric data was collected using Q-Extractive Orbitrap mass spectrometer (Thermo Fisher Scientific, US). The LC-MS raw data was analyzed by MaxQuant software.

Molecular docking

3D modeling of full-length human TRIM7 and MCT4 was conducted by I-TASSER server (https://zhanglab.ccmb.med.umich.edu/I-TASSER/). Next, the SAVES 6.1 server (https://saves.mbi.ucla.edu/), which comprises five evaluation algorithms, was then employed to validate the 3D model, and top-scoring structure was selected for molecular docking analysis. TRIM7 model served as a

ligand and MCT4 was used as the receptor during protein-protein docking via ZDOCK server (https://zdock.wenglab.org/). The binding pattern was visualized and analyzed using PyMOL software.

Single-cell RNA (scRNA-seq) sequencing

Brain tissues were harvested from three experimental groups: naïve mice (n = 2), EAE mice in the peak phase (n = 3), and EAE mice in the chronic phase (n = 2). Single-nucleus library preparation was performed according to our previous report. Once the extracted nuclei passed the quality test, scRNA-seq libraries were prepared using version 3 Chromium Single Cell 3' Library (10x Genomics). Sequencing was performed on Illumina NovaSeq 6000 instrument (Genergy Inc.). CellRanger (version 4.0.0) was used to process raw sequencing data. Cells with more than 10% mitochondrial unique molecular identifier (UMI) or less than 200 genes/cell were excluded from the downstream analysis. Normalization, dimensionality reduction, and clustering of single cells were processed via the Seurat package in R (V4.3.0). Sequencing data have been deposited into the Gene Expression Omnibus (GEO) under the accession number GSE263883.

Western blotting

Cells were lysed in RIPA lysis buffer supplemented with protease and phosphorylase inhibitor (TargetMol, Shanghai, China). Supernatant was collected by centrifuging under 12,000 rpm for 15 min. Whole cell lysates or immunoprecipitates obtained from IP were then separated by electrophoresis on a 10–15% SDS-PAGE gel, and then transferred to a PVDF membranes. Non-specific binding was then blocked in 5% skimmed milk for 1 h at room temperature before incubation with primary antibodies (outlined in Table S3) at 4 °C overnight and incubation with HRP-conjugated secondary antibodies for 1 h. Signals were detected with enhanced chemiluminescence (ECL) kit (Mishu Bio, Xi'an, China) and membranes were visualized with ECL detection system (Tanon4600, Shanghai, China). Quantification of protein band was assessed using Image J software (version 1.53t).

Statistical analysis

GraphPad Prism 8.0 was used for statistical analysis. Data are represented as the mean ± SEM of at least three independent biological replicates in all figures. Data are represented as the mean ± SEM. Data were analyzed for significance using Student's t-test (two groups) or one-way ANOVA with Dunnett's post hoc test (multiple groups). A P value < 0.05 was considered a statistically significant difference.

Abbreviations

BBB	Blood–brain barrier
BSA	Bovine serum albumin
CHCA	α-cyano-4-hydroxy-cinnamic acid
CNS	Central nervous system
DAPI	4',6-diamidino-2-phenylindole
EAE	Experimental autoimmune encephalomyelitis
ECL	Enhanced chemiluminescence
EdU	5-ethynyl-2'-deoxyuridine
GEO	Gene Expression Omnibus
H&E	Hematoxylin and eosin
HRP	Horseradish peroxidase
i.c.v.	Intracerebroventricular
i.p.	Intraperitoneally
IP	Immunoprecipitation
LFB	Luxol fast blue
MCT	Monocarboxylate transporter
$MOG_{35–55}$	Myelin oligodendrocyte glycoprotein peptide 35–55
MS	Multiple sclerosis
NMOSD	Neuromyelitis optica spectrum disorders
p.i.	Post-immunization
PBS	Phosphate buffer saline
PTMs	Post-translational modifications
qRT-PCR	Quantitative real-time polymerase chain reaction
RIPA	Radio-immunoprecipitation assay

Supplementary Information

The online version contains supplementary material available at https://doi.org/10.1186/s12974-025-03453-z.

Supplementary Material 1

Acknowledgements

We thank Shanghai Bioprofile Biotechnology Co., Ltd for mass spectrometry and bioinformatics analysis. We thank Zhaoqiang Qian, Qiangqiang Wei and Lifang Zheng from Laboratory Animal Center of Shaanxi Normal University for their support and assistance in animal feeding, management and experiment.

Author contributions

Conceptualization, L.T.Y; Methodology, L.T.Y, T.T.C, X.Z, Y.Y, Q.Z and Y.L.Z; Validation, L.T.Y and C.Q.H; Investigation, C.Q.H, X.W.C, M.R.S, J.Z, Y.X.X and R.Y.Z; scRNA-seq data analysis: Z.F and Y.G; Data Curation, L.T.Y and C.Q.H; Writing–Original Draft Preparation, L.T.Y; Writing– Review & Editing, C.Q.H; Supervision, Y.P.Y; Funding Acquisition, Y.P.Y.

Funding

This work was supported by National Natural Science Foundation of China (No. 82471381, 82071348), Natural Science Basic Research Program of Shaanxi (No. 2023-JC-JQ-64).

Data availability

No datasets were generated or analysed during the current study.

Declarations

Ethical approval

The study was conducted in accordance with the Declaration of Helsinki, and approved by the Institutional Review Board of Shaanxi Normal university (Permit Number: 2024 – 179).

Consent for publication

Not applicable.

Competing interests

The authors declare no competing interests.

Received: 21 March 2025 / Accepted: 22 April 2025
Published online: 30 April 2025

References

1. Verkhratsky A, Butt A, Li B, Illes P, Zorec R, Semyanov A, Tang Y, Sofroniew MV. Astrocytes in human central nervous system diseases: a frontier for new therapies. Signal Transduct Target Therapy. 2023;8:396.
2. Escartin C, Galea E, Lakatos A, O'Callaghan JP, Petzold GC, Serrano-Pozo A, Steinhäuser C, Volterra A, Carmignoto G, Agarwal A, et al. Reactive astrocyte nomenclature, definitions, and future directions. Nat Neurosci. 2021;24:312–25.
3. Lee H-G, Wheeler MA, Quintana FJ. Function and therapeutic value of astrocytes in neurological diseases. Nat Rev Drug Discovery. 2022;21:339–58.
4. Moulson AJ, Squair JW, Franklin RJM, Tetzlaff W, Assinck P. Diversity of reactive astrogliosis in CNS pathology: heterogeneity or plasticity?? Front Cell Neurosci. 2021;15:703810.
5. Theophanous S, Sargiannidou I, Kleopa KA. Glial cells as key regulators in neuroinflammatory mechanisms associated with multiple sclerosis. Int J Mol Sci. 2024;25:9588.
6. Ponath G, Park C, Pitt D. The role of astrocytes in multiple sclerosis. Front Immunol. 2018;9:217.
7. Mora P, Chapouly C. Astrogliosis in multiple sclerosis and neuro-inflammation: what role for the Notch pathway? Front Immunol. 2023;14:1254586.
8. Takahashi S. Neuroprotective function of high glycolytic activity in astrocytes: Common roles in stroke and neurodegenerative diseases. In international journal of molecular sciences, vol. 22; 2021.
9. Afzal R, Dowling JK, McCoy CE. Impact of exercise on immunometabolism in multiple sclerosis. J Clin Med 2020; 9.
10. Mi Y, Qi G, Vitali F, Shang Y, Raikes AC, Wang T, Jin Y, Brinton RD, Gu H, Yin F. Loss of fatty acid degradation by astrocytic mitochondria triggers neuroinflammation and neurodegeneration. Nat Metabolism. 2023;5:445–65.
11. Yang L, Hu C, Chen X, Zhang J, Feng Z, Xiao Y, He W, Cui T, Zhang X, Yang Y, et al. Upregulated expression of ubiquitin ligase TRIM21 promotes PKM2 nuclear translocation and astrocyte activation in experimental autoimmune encephalomyelitis. eLife. 2024;13:RP98181.
12. Xue D, Wei C, Zhou Y, Wang K, Zhou Y, Chen C, Li Y, Sheng L, Lu B, Zhu Z, et al. TRIOL inhibits rapid intracellular acidification and cerebral ischemic injury: the role of glutamate in neuronal metabolic reprogramming. ACS Chem Neurosci. 2022;13:2110–21.
13. Hirayama Y, Le HPN, Hashimoto H, Ishii I, Koizumi S, Anzai N. Preconditioning-induced facilitation of lactate release from astrocytes is essential for brain ischemic tolerance. eneuro 2024, 11:ENEURO.0494-0423.2024.
14. Wu Y, Gao R, Huang Q, Huang C, Wang L, Lin L, He G, Wu K, Liu X, Liu X, Liu L. Lactate supplementation after hypoglycemia alleviates cognitive dysfunction induced by recurrent non-severe hypoglycemia in diabetic mice. Exp Neurol. 2025;383:115037.
15. Ru Y, Yan X, Zhang B, Song L, Feng Q, Ye C, Zhou Z, Yang Z, Li Y, Zhang Z et al. C-terminal glutamine acts as a C-degron targeted by E3 ubiquitin ligase TRIM7. Proceedings of the National Academy of Sciences: 2022, 119:e2203218119.
16. Chen Q, Zhang T, Zeng R, Zhang K, Li B, Zhu Z, Ma X, Zhang Y, Li L, Zhu J, Zhang G. The E3 ligase TRIM7 suppresses the tumorigenesis of gastric cancer by targeting SLC7A11. Sci Rep. 2024;14:6655.
17. Nijland PG, Michailidou I, Witte ME, Mizee MR, van der Pol SMA, van het Hof B, Reijerkerk A, Pellerin L, van der Valk P, de Vries HE, van Horssen J. Cellular distribution of glucose and monocarboxylate transporters in human brain white matter and multiple sclerosis lesions. Glia. 2014;62:1125–41.
18. Du L, Lin L, Li Q, Liu K, Huang Y, Wang X, Cao K, Chen X, Cao W, Li F, et al. IGF-2 preprograms maturing macrophages to acquire oxidative Phosphorylation-Dependent Anti-inflammatory properties. Cell Metabol. 2019;29:1363–e13751368.
19. Wheeler MA, Clark IC, Tjon EC, Li Z, Zandee SEJ, Couturier CP, Watson BR, Scalisi G, Alkwai S, Rothhammer V, et al. MAFG-driven astrocytes promote CNS inflammation. Nature. 2020;578:593–9.
20. Yang J, Hu X, Wang Y, Liu W, Zhang M, Zhang A, Ni B. Identification of the shared gene signatures and molecular mechanisms between multiple sclerosis and non-small cell lung cancer. Front Immunol. 2023;14:1180449.
21. Hendrickx DAE, van Scheppingen J, van der Poel M, Bossers K, Schuurman KG, van Eden CG, Hol EM, Hamann J, Huitinga I. Gene expression profiling of multiple sclerosis pathology identifies early patterns of demyelination surrounding chronic active lesions. Front Immunol. 2017;8:1810.
22. Brambilla R. The contribution of astrocytes to the neuroinflammatory response in multiple sclerosis and experimental autoimmune encephalomyelitis. Acta Neuropathol. 2019;137:757–83.
23. Kaushik DK, Bhattacharya A, Mirzaei R, Rawji KS, Ahn Y, Rho JM, Yong VW. Enhanced glycolytic metabolism supports transmigration of brain-infiltrating macrophages in multiple sclerosis. J Clin Invest. 2019;129:3277–92.
24. Chatterjee P, Bhowmik D, Roy SS. A systemic analysis of monocarboxylate transporters in ovarian cancer and possible therapeutic interventions. Channels (Austin Tex). 2023;17:2273008.
25. Colombo E, Di Dario M, Menon R, Valente MM, Bassani C, Sarno N, Mazza D, Montini F, Moiola L, Comi G, et al. HNF4α, SP1 and c-myc are master regulators of CNS autoimmunity. J Autoimmun. 2023;138:103053.
26. Kadowaki A, Wheeler MA, Li Z, Andersen BM, Lee H-G, Illouz T, Lee J-H, Ndayisaba A, Zandee SEJ, Basu H et al. CLEC16A in astrocytes promotes mitophagy and limits pathology in a multiple sclerosis mouse model. Nat Neurosci 2025.
27. Peng L, Guangshi L, Wusman LB, Tao L. STK16 promoted colorectal cancer progress in a c-MYC signaling-dependent manner. Mol Med. 2024;30:50.
28. Liu F, Chen J, Li K, Li H, Zhu Y, Zhai Y, Lu B, Fan Y, Liu Z, Chen X, et al. Ubiquitination and deubiquitination in cancer: from mechanisms to novel therapeutic approaches. Mol Cancer. 2024;23:148.
29. Elkjaer ML, Frisch T, Reynolds R, Kacprowski T, Burton M, Kruse TA, Thomassen M, Baumbach J, Illes Z. Molecular signature of different lesion types in the brain white matter of patients with progressive multiple sclerosis. Acta Neuropathol Commun. 2019;7:205.
30. Elkjaer ML, Hartebrodt A, Oubounyt M, Weber A, Vitved L, Reynolds R, Thomassen M, Rottger R, Baumbach J, Illes Z. Single-Cell Multi-Omics map of cell Type-Specific mechanistic drivers of multiple sclerosis lesions. Neurol Neuroimmunol Neuroinflamm. 2024;11:e200213.
31. Nijland PG, Molenaar RJ, van der Pol SMA, van der Valk P, van Noorden CJF, de Vries HE, van Horssen J. Differential expression of glucose-metabolizing enzymes in multiple sclerosis lesions. Acta Neuropathol Commun. 2015;3:79.
32. Braga A, Chiacchiaretta M, Pellerin L, Kong D, Haydon PG. Astrocytic metabolic control of orexinergic activity in the lateral hypothalamus regulates sleep and wake architecture. Nat Commun. 2024;15:5979.
33. Wang Y, Qin L, Chen W, Chen Q, Sun J, Wang G. Novel strategies to improve tumour therapy by targeting the proteins MCT1, MCT4 and LAT1. Eur J Med Chem. 2021;226:113806.
34. Zhao M, Huang C, Yang L, Pan B, Yang S, Chang J, Jin Y, Zhao G, Yue D, Qie S, Ren L. SYVN1-mediated ubiquitylation directs localization of MCT4 in the plasma membrane to promote the progression of lung adenocarcinoma. Cell Death Dis. 2023;14:666.
35. Mei L, Zheng Y-M, Song T, Yadav VR, Joseph LC, Truong L, Kandhi S, Barroso MM, Takeshima H, Judson MA, Wang Y-X. Rieske iron-sulfur protein induces FKBP12.6/RyR2 complex remodeling and subsequent pulmonary hypertension through NF-κB/cyclin D1 pathway. Nat Commun. 2020;11:3527.
36. Guo Q, Jin Y, Chen X, Ye X, Shen X, Lin M, Zeng C, Zhou T, Zhang J. NF-κB in biology and targeted therapy: new insights and translational implications. Signal Transduct Target Therapy. 2024;9:53.
37. Zhong W, Wu K, Long Z, Zhou X, Zhong C, Wang S, Lai H, Guo Y, Lv D, Lu J, Mao X. Gut dysbiosis promotes prostate cancer progression and docetaxel resistance via activating NF-κB-IL6-STAT3 axis. Microbiome. 2022;10:94.
38. Chan KI, Zhang S, Li G, Xu Y, Cui L, Wang Y, Su H, Tan W, Zhong Z. MYC oncogene: A druggable target for treating cancers with natural products. Aging Dis. 2024;15:640–97.
39. Zhang S, Xu W, Wang H, Cao M, Li M, Zhao J, Hu Y, Wang Y, Li S, Xie Y, et al. Inhibition of CREB-mediated ZO-1 and activation of NF-κB-induced IL-6 by colonic epithelial MCT4 destroys intestinal barrier function. Cell Prolif. 2019;52:e12673.
40. Hu X, Liu Z, Duan X, Han X, Yuan M, Liu L, Xia X, Li N, Qin J, Wang Y. Blocking MCT4 sumoylation inhibits the growth of breast cancer cells. Mol Carcinog. 2021;60:702–14.
41. Kolla S, Ye M, Mark KG, Rapé M. Assembly and function of branched ubiquitin chains. Trends Biochem Sci. 2022;47:759–71.
42. Fan W, Mar KB, Sari L, Gaszek IK, Cheng Q, Evers BM, Shelton JM, Wight-Carter M, Siegwart DJ, Lin MM, Schoggins JW. TRIM7 inhibits enterovirus replication and promotes emergence of a viral variant with increased pathogenicity. Cell. 2021;184:3410–e34253417.
43. Giraldo MI, Xia H, Aguilera-Aguirre L, Hage A, van Tol S, Shan C, Xie X, Sturdevant GL, Robertson SJ, McNally KL, et al. Envelope protein ubiquitination drives entry and pathogenesis of Zika virus. Nature. 2020;585:414–9.
44. Jin J, Lu Z, Wang X, Liu Y, Han T, Wang Y, Wang T, Gan M, Xie C, Wang J, Yu B. E3 ubiquitin ligase TRIM7 negatively regulates NF-kappa B signaling pathway by degrading p65 in lung cancer. Cell Signal. 2020;69:109543.
45. Zhou C, Zhang Z, Zhu X, Qian G, Zhou Y, Sun Y, Yu W, Wang J, Lu H, Lin F et al. N6-Methyladenosine modification of the TRIM7 positively regulates

tumorigenesis and chemoresistance in osteosarcoma through ubiquitination of BRMS1. eBioMedicine: 2020, 59.
46. Zhu L, Qin C, Li T, Ma X, Qiu Y, Lin Y, Ma D, Qin Z, Sun C, Shen X, et al. The E3 ubiquitin ligase TRIM7 suppressed hepatocellular carcinoma progression by directly targeting Src protein. Cell Death Differ. 2020;27:1819–31.
47. Chakraborty A, Diefenbacher ME, Mylona A, Kassel O, Behrens A. The E3 ubiquitin ligase Trim7 mediates c-Jun/AP-1 activation by Ras signalling. Nat Commun. 2015;6:6782.
48. Yan Y, Ding X, Li K, Ciric B, Wu S, Xu H, Gran B, Rostami A, Zhang G-X. CNS-specific therapy for ongoing EAE by Silencing IL-17 pathway in astrocytes. Mol Ther. 2012;20:1338–48.
49. Ding X, Yan Y, Li X, Li K, Ciric B, Yang J, Zhang Y, Wu S, Xu H, Chen W, et al. Silencing IFN-γ binding/signaling in astrocytes versus microglia leads to opposite effects on central nervous system autoimmunity. J Immunol. 2015;194:4251–64.

Publisher's note